Electronic Supplementary Material (ESI) for Physical Chemistry Chemical Physics.

Supplementary Information

Degradation Paths of Manganese-Based MOF Materials in a Model Oxidative Environment: a Computational Study

Elena V. Khramenkova,[a] Mikhail V. Polynski,[a*] Alexander V. Vinogradov,[a] Evgeny A. Pidko[a,b*]

[a] TheoMAT group, International Laboratory "Solution Chemistry of Advanced Materials and Technologies", ITMO University, Lomonosova str. 9, St. Petersburg 191002, Russia, E-mail: polynskimikhail@gmail.com

[b] Inorganic Systems Engineering group, Department of Chemical Engineering, Faculty of Applied Sciences, Delft University of Technology, Van der Maasweg 9, 2629 HZ Delft, The Netherlands, E-mail: E.A.Pidko@tudelft.nl

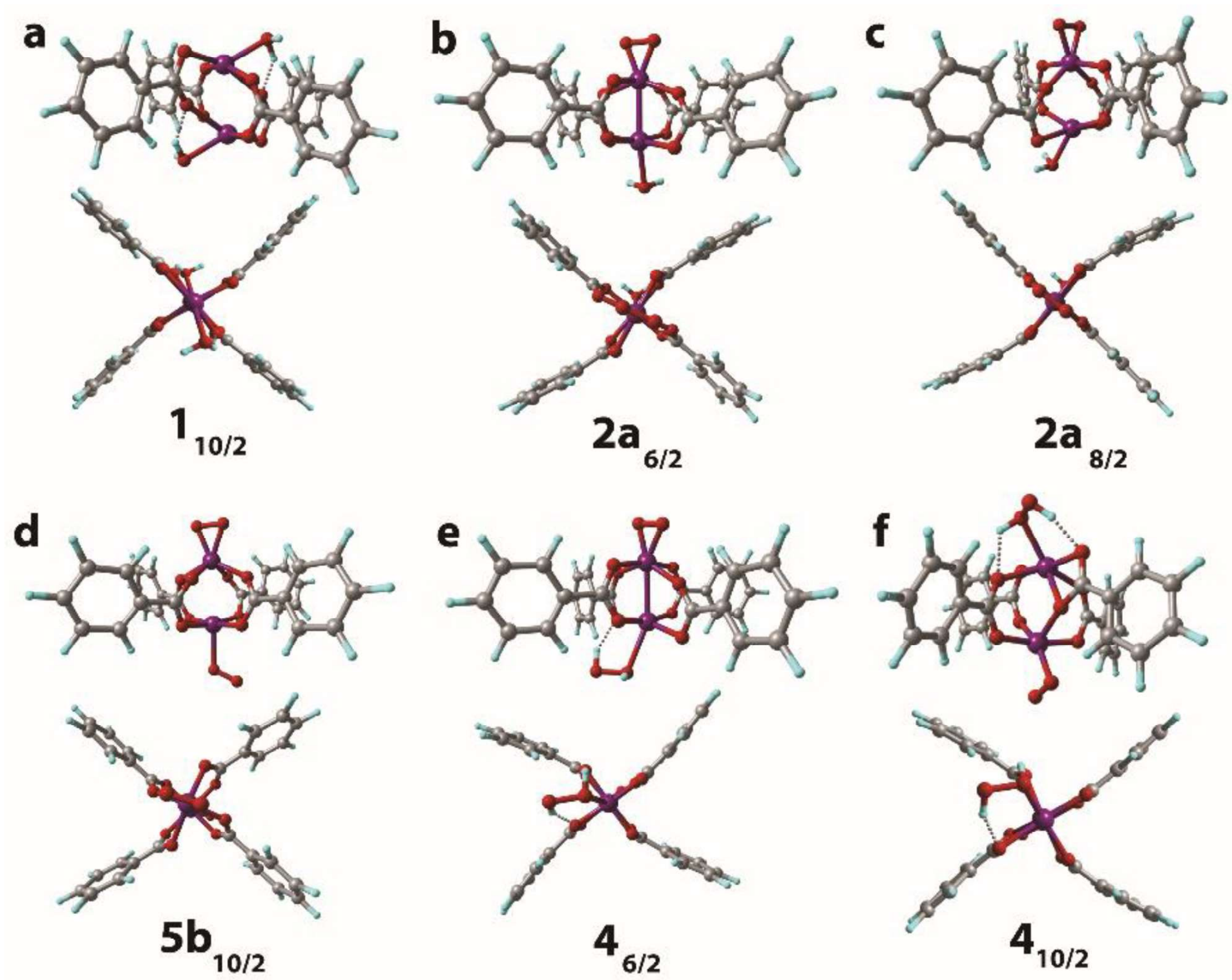

Figure S1. The optimized at the PBE-D3/6-31G(d,p) geometries (front and side views) of $\mathbf{1_{10/2}}$ (a), $\mathbf{2a_{6/2}}$ (b), $\mathbf{2a_{8/2}}$ (c), $\mathbf{5b_{10/2}}$ (d), $\mathbf{4_{6/2}}$ (e), $\mathbf{4_{10/2}}$ (f) complexes with fixed para-H atoms.

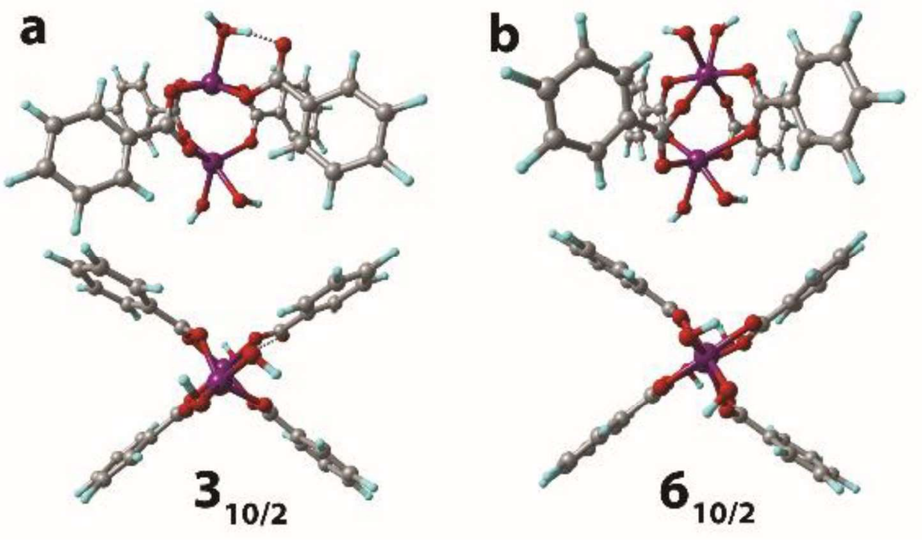

Figure S2. The optimized at the PBE-D3/6-31G(d,p) geometries (front and side views) of the $\mathbf{3_{10/2}}$ (a), $\mathbf{6_{10/2}}$ (b) complexes with fixed para-H atoms.

The steric tension imposed in the structures during the constrained optimization made the optimization procedure unstable in several cases preventing the reach of the minima with the default convergence criteria. The total energy changes were less than 1 kJ/mol prior the instability points in the all observed instability cases (i.e., the instability was encountered in the tail region of the geometry optimization procedure). Therefore, the structures in the pre-instability points were considered as well-converged.

Table S1. Binding energies corresponding to **2a**$_{6/2}$, **2a**$_{8/2}$, **4**$_{6/2}$, **4**$_{10/2}$, **5b**$_{10/2}$ complexes formation as computed at the PBE-D3/6-311++G(d,p)//PBE-D3/6-31G(d,p) level of theory with fixed para-H-atoms. Energies are given in kJ/mol.

2a$_{6/2}$	9	**2a**$_{8/2}$	-51	**4**$_{6/2}$	-2	**4**$_{10/2}$	-9	**5b**$_{10/2}$	-5

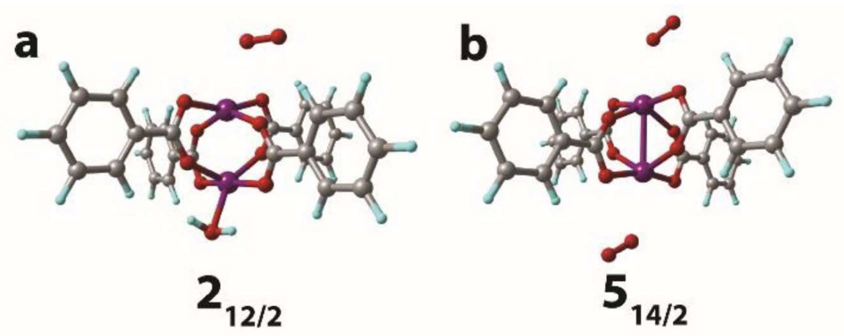

Figure S3. The optimized at the PBE-D3/6-31G(d,p) level geometries (side views) of the $O_2[Mn_2(PhCOO)_4]H_2O$ (a) and $O_2[Mn_2(PhCOO)_4]O_2$ (b) complexes in s = 12/2 and 14/2 spin states respectively.

Table S2. The Mulliken spin density values on the Mn sites in $L[Mn_2(PhCOO)_4]L$ complexes computed at the PBE-D3/6-31G(d,p) level of theory and the corresponding bonding modes. The spin density values in the bound O_2 species parentheses.

	Mn-H_2O	Mn-H_2O
1$_{6/2}$	3.16	3.16
1$_{8/2}$	3.28	4.49
1$_{10/2}$	4.80	4.80

	Mn-O_2	Mn-H_2O_2
4$_{6/2}$	2.35-(0.15, 0.15)	3.29
4$_{8/2}$	2.91-(0.11, 0,11)	4.63
4$_{10/2}$	3.88-(0.42, 0.61)	4.74

	Mn-O_2	Mn-H_2O
2$_{6/2}$	2.33-(0.15, 0.15)	3.32
2$_{8/2}$	2.94-(0.11, 0.10)	4.62
2$_{10/2}$	3.56-(0.70, 0.82)	4.67
2$_{12/2}$	4.78-(1.02, 0.98)	4.80

	Mn-O_2	Mn-O_2
5$_{6/2}$	3.01-(0.71, 0.86)	2.45-(-0.35, -0.59)
5$_{8/2}$	3.61-(0.38, 0.46)	3.84-(-0.27, -0.27)
5$_{10/2}$	3.83-(0.78, 0.93)	3.93-(0.15, 0.15)
5$_{14/2}$	4.79-(0.98, 1.02)	4.79-(0.98, 1.02)

	Mn-H_2O_2	Mn-H_2O
3$_{6/2}$	3.14	3.17
3$_{10/2}$	4.77	4.79

	Mn-H_2O_2	Mn-H_2O_2
6$_{6/2}$	3.14	3.14
6$_{10/2}$	4.77	4.77

Table S3. The Mulliken spin density values on the Mn sites in L[$Mn_2(PhCOO)_4$]L complexes (S = 6/2 and 10/2) in oxidation-induced hydrolysis as computed at the PBE-D3/6-31G(d,p) level of theory.

Initial State Mn1/Mn2			Transition State Mn1/Mn2			Final State Mn1/Mn2			Hydrolysis Mn1/Mn2		
$\mathbf{6}_{6/2}$	3.14	3.14	$\mathbf{TS}_{6/2}$	3.12	2.76	$\mathbf{7}_{6/2}$	3.62	2.33	$\mathbf{8}_{6/2}$	3.55	2.17
$\mathbf{6}_{10/2}$	4.78	4.78	$\mathbf{TS}_{10/2}$	4.76	4.52	$\mathbf{7}_{10/2}$	4.71	3.90	$\mathbf{8}_{10/2}$	4.73	3.88

Table S4. The Mulliken charge values on the Mn sites in L[$Mn_2(PhCOO)_4$]L complexes computed at the PBE-D3/6-31G(d,p) level of theory.

	$Mn\text{-}H_2O$	$Mn\text{-}H_2O$
$\mathbf{1}_{6/2}$	0.89	0.89
$\mathbf{1}_{8/2}$	0.87	0.84
$\mathbf{1}_{10/2}$	0.99	0.99

	$Mn\text{-}O_2$	$Mn\text{-}H_2O_2$
$\mathbf{4}_{6/2}$	1.12	0.92
$\mathbf{4}_{8/2}$	1.25	1.04
$\mathbf{4}_{10/2}$	1.17	1.01

	$Mn\text{-}O_2$	$Mn\text{-}H_2O$
$\mathbf{2}_{6/2}$	1.12-	0.91
$\mathbf{2}_{8/2}$	1.25	1.02
$\mathbf{2}_{10/2}$	1.04	0.96
$\mathbf{2}_{12/2}$	0.99	0.98

	$Mn\text{-}O_2$	$Mn\text{-}O_2$
$\mathbf{5}_{6/2}$	1.03	1.07
$\mathbf{5}_{8/2}$	1.12	1.19
$\mathbf{5}_{10/2}$	1.08	1.17
$\mathbf{5}_{14/2}$	1.01	1.07

	$Mn\text{-}H_2O_2$	$Mn\text{-}H_2O$
$\mathbf{3}_{6/2}$	0.91	0.89
$\mathbf{3}_{10/2}$	1.02	0.99

	$Mn\text{-}H_2O_2$	$Mn\text{-}H_2O_2$
$\mathbf{6}_{6/2}$	0.91	0.91
$\mathbf{6}_{10/2}$	1.01	1.01

Table S5. The Mulliken charge values on the Mn sites in L[$Mn_2(PhCOO)_4$]L complexes (S = 6/2 and 10/2) in oxidation-induced hydrolysis as computed at the PBE-D3/6-31G(d,p) level of theory.

Initial State Mn1/Mn2			Transition State Mn1/Mn2			Final State Mn1/Mn2			Hydrolysis Mn1/Mn2		
$\mathbf{6}_{6/2}$	0.91	0.91	$\mathbf{TS}_{6/2}$	0.96	0.97	$\mathbf{7}_{6/2}$	1.09	1.05	$\mathbf{8}_{6/2}$	1.10	1.06
$\mathbf{6}_{10/2}$	1.01	1.01	$\mathbf{TS}_{10/2}$	1.00	1.11	$\mathbf{7}_{10/2}$	1.03	1.16	$\mathbf{8}_{10/2}$	1.02	1.15

Table S6. Binding energies corresponding to the L[Mn_2BzO_4]L complexes formation as computed at the PBE-D3/6-31G(d,p) level of theory. Energies are given in kJ/mol.

$\mathbf{2}_{6/2}$	-44	$\mathbf{5}_{6/2}$	-7	$\mathbf{3}_{6/2}$	6	$\mathbf{4}_{6/2}$	-49
$\mathbf{2}_{8/2}$	-79	$\mathbf{5}_{8/2}$	-41	$\mathbf{3}_{10/2}$	-7	$\mathbf{4}_{8/2}$	-80
$\mathbf{2}_{10/2}$	11	$\mathbf{5}_{10/2}$	-23	$\mathbf{6}_{6/2}$	-1	$\mathbf{4}_{10/2}$	-34
$\mathbf{2}_{12/2}$	76	$\mathbf{5}_{14/2}$	153	$\mathbf{6}_{10/2}$	-14	$\mathbf{1}_{10/2}$	-149